Corrosion mechanisms in aqueous solutions containing dissolved H2S. Part 2: Model of the cathodic reactions on a 316L stainless steel rotating disc electrode

Bernard Tribollet, Jean Kittel, A. Meroufel, F. Ropital, F Grojean, Eliane Sutter, F. Grosjean

▶ **To cite this version:**

Bernard Tribollet, Jean Kittel, A. Meroufel, F. Ropital, F Grojean, et al.. Corrosion mechanisms in aqueous solutions containing dissolved H2S. Part 2: Model of the cathodic reactions on a 316L stainless steel rotating disc electrode. Electrochimica Acta, 2014, 124, pp.46-51. 10.1016/j.electacta.2013.08.133 . hal-01017493v2

HAL Id: hal-01017493
https://hal.sorbonne-universite.fr/hal-01017493v2

Submitted on 20 Dec 2019

HAL is a multi-disciplinary open access archive for the deposit and dissemination of scientific research documents, whether they are published or not. The documents may come from teaching and research institutions in France or abroad, or from public or private research centers.

L'archive ouverte pluridisciplinaire **HAL**, est destinée au dépôt et à la diffusion de documents scientifiques de niveau recherche, publiés ou non, émanant des établissements d'enseignement et de recherche français ou étrangers, des laboratoires publics ou privés.

Corrosion mechanisms in aqueous solutions containing dissolved H_2S. Part 2: Model of the cathodic reactions on a 316L rotating disc electrode.

B. Tribollet[1*], J. Kittel[2], A. Meroufel[2,3], F. Ropital[2], F. Grojean[2], E.M.M. Sutter[1]

[1] *Laboratoire Interfaces et Systèmes Electrochimiques, UPR 15 du CNRS, UPMC, 75252 Paris Cedex 05, France.*
[2] *IFP Energies nouvelles, Rond-point de l'échangeur de Solaize BP3, 69360 Solaize, France.*
[3.] *Corrosion Department, Seawater Desalination Research Institute;Saline Water Conversion Corporation, P.O. Box 8382, Al Jubail 31951 ; Kingdom of Saudi Arabia.*

Abstract

In H_2S containing solutions, the reduction of protons with a buffer effect contributing to the transport of protons at the steel surface, is not sufficient to explain the cathodic polarization curves. An additional electrochemical reaction was observed and was attributed to a direct H_2S reduction. A numerical model is presented with these hypotheses and a good agreement is found with the experimental data presented in a previous paper. With this model it is also possible to present the concentration profiles of the different species involved in the cathodic process.

1. Introduction

Corrosion in weak acid solutions often represents a more complex situation than in strong acids. It is relatively well admitted that corrosion in weak acids is usually enhanced in comparison with diluted strong acids at the same pH. A simple explanation to this fact lies in the carrier of reducible proton (H^+). In a strong acid solution, all the protons are already dissociated. Consequently, pH is a good indicator of the oxidizing power of the solution. On the other hand, a weak acid solution of similar pH still contains the same amount of H^+, but also a reservoir of protons in the form of undissociated weak acid molecules. The oxidizing power is thus accounted for by both pH and the concentration of weak acid, with immediate consequences on the intensity of the cathodic reaction at a given potential. In acid solution, H^+ reduction is often the major source of cathodic current. In a weak acid solution, this cathodic reaction is both fed by H^+ diffusion from the bulk, but also by the diffusion of the weak acid and its subsequent dissociation, in a so called buffer effect. The increase of cathodic current associated with this buffer effect is therefore seen as soon as a H^+ diffusion limitation is reached, and the higher the weak acid concentration is, the higher the increase of cathodic current. However, in order to explain the increase of cathodic current, the hypothesis of electroactivity of the weak acid is also often proposed. The direct reduction of the weak acid is then mathematically added to proton reduction, thus increasing the total cathodic current density.

Although the differences between those two mechanisms might seem subtle, major differences have to be pointed out. The buffer effect arises purely from chemical equilibria and kinetics, without potential dependence. It is therefore necessarily always a contributor. However, this contribution starts only in the potential region where H^+ reduction is under mass transport control: the weak acid then acts as a buffer, and is transported from the bulk to the electrode surface, where it dissociates to generate H^+ in situ. As a consequence, cathodic polarization curves are expected to remain unchanged in the H^+ charge transfer region, while

the diffusion limited plateau must be increased with an amplitude corresponding to diffusion of the weak acid.
On the contrary, a direct reduction has a strong dependence on potential. It may or it may not be found in the potential range of H^+ reduction, depending on the nature of the electrode, the nature of the weak acid and its concentration. When the contribution of weak acid reduction is not negligible, it thus presents its own current – potential characteristics with charge transfer and mass transfer limited regions, which are superimposed to H^+ reduction, enhanced by the buffer effect which is still present. If both reduction reactions have distinct potential regions and not too dissimilar current densities, two distinct electrochemical waves should be observed in the current – potential curves.

In oil and gas environments, three major weak acids are encountered: from the strongest to the weakest, organic acids, with acetic acid (CH_3COOH) as the main component, carbonic acid (H_2CO_3) and hydrosulfuric acid (H_2S). While it is known from decades that these acids strongly enhance the corrosion rates of mild steel [1-13] the level of understanding differs widely between them. CO_2 corrosion has probably benefited the widest and earliest investigations, and it is known from long that the increase of corrosion rate is associated with an increase of cathodic current density [4,5,7,9-12]. While direct reduction of H_2CO_3 remained the most often cited mechanism until the late 2000's, a recent consensus seems adopted on the buffer effect which was first proposed in 1974 [12]. This mechanism was recently confirmed by a reactive transport model showing that no additional reduction reaction was necessary to describe cathodic reactions in CO_2 solutions [14]. Similarly, recent studies on acetic acid corrosion also showed that a direct reduction was not likely [15], also confirming older thoughts [3].
On the other hand, studies on H_2S corrosion were mainly focused on anodic mechanism or on the formation of FeS scale formation [8,16-19]. Electrochemical aspects of H_2S benefited much less investigations, though it was found to have strong impact on the cathodic current density [1,8,20]. Recent electrochemical investigations were thus performed using well controlled hydrodynamic systems and show that H_2S contribution might not fully be explained by a buffer effect [21,22].
In Part 1 of this paper, an electrochemical model for the cathodic reactions in H_2S solutions was proposed [21]. A buffer behaviour similar to CO_2 was first considered, where H_2S contributes through its dissociation reactions as an additional source of protons at the corroding surface:

$$H_2S \leftrightarrow H^+ + HS^- \quad (1)$$
$$HS^- \leftrightarrow H^+ + S^{2-} \quad (2)$$

As in the case of CO_2 [23], it is not postulated that these reactions always stand at thermodynamic equilibrium. It could thus be necessary to consider the chemical kinetics expressions:

$$R_1 = k_1 C_{H_2S} - k_{-1} C_{HS^-} C_{H^+} \quad (3)$$
$$R_2 = k_2 C_{HS^-} - k_{-2} C_{S^{2-}} C_{H^+} \quad (4)$$

where R_1, k_1 and k_{-1} are respectively the rates of the reaction and the forward and backward kinetic constants for H_2S dissociation (Reaction (1)), and where R_2, k_2 and k_{-2} have the same meaning for HS^- dissociation (Reaction (2)). Although the kinetic rate constants for these

reactions are not well documented in the literature, it is often postulated that the dissociation of H_2S is much faster than for CO_2 [24].
As it was also shown in [21], the buffer effect is not sufficient to explain the experimental cathodic curves: an additional electrochemical reaction was observed at higher cathodic potential, which could not be represented by the proton reduction after weak acid transport and dissociation. The hypothesis of a direct reduction reaction was then considered as proposed by Bolmer [1]:

$$H_2S + e^- \quad \leftrightarrow \quad HS^- + \frac{1}{2}H_2 \qquad (5)$$

The reaction order of this last reaction was experimentally determined in [21] and a value of 0.5 was found as for the proton.
Finally the expression of the current density for the reaction (3) was obtained after the determination of the Tafel slope:

$$J_{H_2S} = k_{H_2S} C_{H_2S}^{0.5}(0) 10^{\frac{-E}{b_{c,H_2S}}} \qquad (6)$$

where k_{H_2S} is the cathodic rate constant of H_2S reduction, $C_{H_2S}(0)$ is the H_2S concentration at the electrode surface, E is the electrode potential, and b_{c,H_2S} is the cathodic Tafel slope equal to 145±10mV (1).

2 Governing equations

Generally, the solution under investiagation contains different ions as Na^+, $SO4^{--}$, Cl^- and then in this approach the migration is neglected. The migration can play a significant role only in pure water which is not realistic in oil and gas industry.
The governing equations of the system are the mass balance equations expressed for each species *i* of the model. These equations can be written according to:

$$-D_i \frac{\partial^2 C_i}{\partial x^2} + V_x \frac{\partial C_i}{\partial x} = R_i \qquad (7)$$

with Di the diffusion coefficient of species *i*, C_i its concentration, V_x the convective transport rate in the direction normal to the electrode surface, and R_i the homogeneous production rate, determined from (3) and (4) with the following relations:

$$R_{H^+} = R_1 + R_2 \qquad (8)$$
$$R_{H_2S} = -R_1 \qquad (9)$$
$$R_{HS^-} = R_1 - R_2 \qquad (10)$$
$$R_{S^{2-}} = -R_2 \qquad (11)$$

According to Levich [25], the convective term for a rotating disc electrode can be expressed as:

$$V_x = -0.51 \upsilon^{-1/2} \omega^{3/2} x^2 \qquad (12)$$

Where ν is the kinematic viscosity of the solution, ω is the angular rotation speed of the electrode, and x is the normal distance to the electrode surface.
The complete system is described by a set of four coupled non linear differential equations (7), to solve it, the boundary conditions at the interface and in the bulk of the solution must be defined.

2.1 Boundary conditions in the bulk of the solution:

Far from the electrode, it is reasonable to consider that thermodynamic equilibrium is reached. Thus for a given pH and a given partial pressure of H_2S (P_{H_2S}), the bulk concentration can easily be calculated as:

$$C_{H_2S} = H_{H_2S} P_{H_2S} \tag{13}$$

$$C_{HS^-} = K_1 \frac{C_{H_2S}}{C_{H^+}} \tag{14}$$

$$C_{S^{2-}} = K_2 \frac{C_{HS^-}}{C_{H^+}} \tag{15}$$

where H_{H_2S} is the Henry's constant for H_2S, and K_1 and K_2 are respectively the equilibrium constant of Reaction (1) and Reaction (2).
It appears that $C_{S^{2-}} = K_1.K_2 \frac{C_{H_2S}.C_{HS^-}}{C_{H^+}^2}$ and the corresponding value is very small, then for the pH value under investigation (pH = 4 and pH = 6, the concentration in S^{2-} is negligible and the homogeneous reaction (2) can be ignored in the present work.

2.2 Boundary conditions at the electrode surface:

At the electrode surface the flux of non electroactive species is necessarily equal to zero:

$$\left.\frac{\partial C_{HS^-}}{\partial x}\right|_{x=0} = \left.\frac{\partial C_{S^{2-}}}{\partial x}\right|_{x=0} = 0 \tag{16}$$

The electroactive species are H^+ and H_2S, then:

$$D_{H_2S} \left.\frac{\partial C_{H_2S}}{\partial x}\right|_{x=0} = J_{H_2S} \tag{17}$$

$$D_{H^+} \left.\frac{\partial C_{H^+}}{\partial x}\right|_{x=0} = J_{H^+} \tag{18}$$

J_{H_2S} is given by the expression (6) and the expression for J_{H^+} is similar and given in [21]. The boundary conditions (17) and (18) linked the concentration at the electrode to the concentration gradient.

3 Numerical solutions

3.1 *Current-potential curves*

Due to the product of concentrations $C_{HS^-}C_{H^+}$ in equation (3) the system is non linear. Only the equilibrium constant K_1 is tabulated but k_1 is unknown and can be determined by comparison between the numerical derivation and the experimental data. The corresponding values k_{-1} is deduced from the values of k_1 ($k_{-1} = K_1/k_1$).
The numerical value for the overall current is:

$$i = F(J_{H_2S} + J_{H^+}) \qquad (19)$$

The dissociation of HS^- is neglected, the system is then reduced to three differential equations with three unknowns and only k_1 must be determined.

The stationary cathodic polarization curves measured with a rotating disc electrode at pH 4 in H_2S saturated (9 mbar) solution is recalled in Figure 1 at 600 rpm. Two waves can be clearly seen and are attributed to the reduction of the proton and to the reduction of H_2S (reaction (5)). For potentials more cathodic than -1 V, a third wave can be observed corresponding to the water reduction and is not considered in the present simulation.
The parameters corresponding to the simulation presented in Figure 1 are given in Table 1. The results of the derivation are also given in Figure 1, a good agreement between the experimental data and the simulation is obtained. The wave corresponding to the H_2S reduction is obtained by taking a value for k_{H_2S} lower than the value of k_{H^+} (see Table 1).
In order to characterize in more details the electrochemical reactions associated with H_2S, additional experiments were performed in [21] with different P_{H_2S} or less acidic solutions. All simulations are obtained with the same set of coefficients (Table 1).
At pH 4 for 9 and 50 mbar of H_2S, the additional contribution to the proton reduction appears on the polarization curves of Figure 2. For 1 mbar only the reduction of the proton appears clearly. As in Figure 1 the agreement between the simulated curves and the experimental data is satisfactory.
At pH 6 for the different concentrations in H_2S, the cathodic contribution of the polarization curves can be attributed to H_2S and to the water reduction. The simulation confirms that the limiting plateau is proportional to the H_2S concentration, but the water reduction is not introduced in the model (Figure 3).
The stationary cathodic polarization curves in the limiting current domain are plotted in Figure 4 for different rotation rates of the electrode at pH 6 and with 50 mbar H_2S. The simulated curves show a good agreement for the kinetic part but a clear discrepancy in the limiting current region. Only the curve at 180 rpm is in agreement with the experimental data.
The limiting cathodic current is plotted versus the square root of the rotation speed in Figure 5. On this figure the simulated points corresponding to the previous curves are reported with a black square, and correspond to a k_1 value of 0.2. The simulated points are below the Levich plot and the corresponding curve is parallel to the Levich curve. To see the effect of k_1 on the simulated results, for the same conditions the current was simulated with a k_1 value of 0.5. Again the corresponding curve is below the Levich curve but always parallel to the Levich curve. The experimental data follow a completely different behaviour, the increase of the current with the rotation speed is much lower than the square root of the rotation speed. To understand the effect of k_1 on the limiting current, in Figure 6 the limiting current corresponding to a rotation speed of 180 rpm for a solution at pH 6 and with 50 mbar H_2S is

plotted versus the k_1 value. Clearly the value of k_1 plays an important role for k_1 around 0.1 and in order to obtain the best agreement on Figure 1 a value of 0.2 was chosen. The homogeneous reaction (1) influences the limiting current if the k_1 value is larger than 0.01. For k_1 value below 0.01 the current follows the Levich law and the homogeneous reaction plays no role on the limiting current value.

3.2 *Concentration profiles*

The previous model needs to derive the concentration field near the electrode for each species involved in the reaction. An example of the concentration variation versus the normal distance of the electrode is given in Figure 7. The distance is dimensionless by using the diffusion layer thickness corresponding to the proton. In Figure 7 it appears clearly than in mixed kinetic for H_2S (potential = - 0.83 V) the concentration at the interface is not zero but at this potential the reduction of H^+ is mass transport limited and the concentration at the interface is zero. It appears also that the concentration gradient of HS^- at the interface is equal to zero in agreement with the boundary conditions.
In Figure 8, the concentration profiles are presented for a potential corresponding to the limiting current of H_2S. In the coordinates used in this figure, the difference between the thickness of the diffusion layer for the proton and for H_2S appears clearly; this difference is obviously due to the difference between the diffusion coefficients of the two species. The HS^- concentration is too small in this representation to be visible on this figure.
Finally, the effect of the forward constant k_1 on the concentration profile of H_2S is represented in Figure 9. In agreement with figure 6, the concentration profile for a k_1 value small enough tends towards the concentration profile without any homogeneous reaction, and for higher values of k_1 the concentration gradient at the interface decreases. It is interesting to notice that the H_2S concentration reaches the bulk concentration at distance 6 or 7 times larger for k_1 equal 0.5 than for k_1 equal 0.001. As consequence for large value of k_1 the numerical integration of the mass balance equation must be performed on a larger distance.

4 Discussion

As shown experimentally in part 1 of this paper [21], and also observed in [22], the hydrogen evolution in an oxygen free solution with dissolved H_2S is different from that observed with dissolved CO_2, even though both dissolved gasses are weak acids with comparable solubility and pKa. In the pH region of interest for oil and gas environments, typically between 4 and 6, the concentration of dissolved acid gases (CO_2 and H_2S) is usually several orders of magnitude higher than the concentration of proton. Electrochemical reactions at the steel surface are then under strong influence of the transport of the weak acids coupled with their dissociation. However, while this reactive transport scheme with proton reduction as unique cathodic contribution was sufficient to describe polarisation curves in carbonic acid solutions, the same model could not be applied satisfactorily with H_2S. As shown by numerical results presented in this paper, the buffer effect is not sufficient to explain cathodic polarization curves measured in solutions with dissolved H_2S. The hypothesis of an additional reduction of H_2S was considered and the numerical curves are in good agreement with the experimental ones. However a discrepancy appears for the variation of the limiting current with the rotation speed, in contradiction with experimental results of [22], obtained with mild steel electrode. Several hypothesis might be proposed to explain this discrepancy. Sulfide adsorbates at the electrode surface might have disturbed the system, inducing areas with distinct electrochemical reactivities. Thus, the additional electrochemical wave might be linked with a second "H_2S modified surface" rather than with, or in addition to, a second electroactive

species. This reaction scheme is also in good agreement with the current understanding of the impact of H_2S on hydrogen charging in steel, considering proton reduction through HS^- adsorbate [26].
Another type of surface disturbance might also explain the experimental variation of the limiting current with the rotation speed. This difference could be due to the fact that the direct corrosion of iron with H_2S and the formation of a corrosion deposit were not taken into account in the present model [18].
Although it is not possible to conclude at this stage, it seems also that these hypotheses strongly depend on the electrode material. While we used stainless steel for its relative inertness for this investigation, carbon steel presents a much greater practical interest, and constitutes the main perspective to this work. In particular, the rapid formation of corrosion scales is expected, constituting a porous diffusion layer. The model could then be modified in order to remove the convective transport contributions, and apply a diffusion layer in the typical range of corrosion scales, from tens of micrometres to millimetres. This will also require taking account of ferrous ions diffusions from the steel surface through the porous layer, and also consider precipitation reactions. This model could then be applied to discuss corrosion under deposit mechanisms as described in [27,28]. Such mechanistic models of CO_2 and H_2S underdeposit corrosion already exist, but they do not incorporate actual understanding of H_2S electrochemistry and reactive transport [19].
Improving the understanding of H_2S corrosion of carbon steel would also be valuable for hydrogen cracking applications, with a better understanding of the impact of adsorbates on hydrogen entry.

5 Conclusion

The contribution of H_2S to cathodic reactions differs from that of CO_2 or acetic acid. In the latter case, proton reduction is the main cathodic reaction, and dissolved CO_2 or acetic acid only contribute to increase the current density in the mass transfer control potential range by a chemical buffer effect. While such buffer effect still holds with H_2S, it is no more sufficient to explain the rise of cathodic current, and the appearance of a second electrochemical wave. A kinetic model, including both a buffer effect and a direct H_2S reduction was proposed in Part 1 of this paper. Numerical resolution was proposed in this paper, and showed good agreement with experimental data obtained on a 316L rotating disc electrode in pH region 4 to 6 and H_2S partial pressure from 1 to 50 mbar.

6 References

[1] P.W. Bolmer, Polarization of iron in H_2S-NaHS buffers, Corrosion 21 (1965) 69-75.
[2] J.L. Crolet, Acid corrosion in wells (CO_2, H_2S): Metallurgical aspects, International Petroleum Exhibition and Technical Symposium of the Society of Petroleum Engineers (SPE10045), Bejing, China, 18-26 March (1982).
[3] J.L. Crolet and M.R. Bonis, The role of acetate ions in CO_2 corrosion, NACE Corrosion/83 paper n°160, Anaheim, CA (USA) 18-22 April (1983).
[4] C. Dewaard and D.E. Milliams, Carbonic-Acid Corrosion of Steel, Corrosion 31 (1975) 177-181.
[5] L.G.S. Gray, B.G. Anderson, M.J. Danysh, and P.R. Tremaine, Mechanisms of carbon steel corrosion in brines containing dissolved carbon dioxide at pH 4, NACE Corrosion/89 paper n°464, New Orleans, LO (USA) 17-21 April (1989).

[6] K.L.J. Lee and S. Nesic, The effect of trace amount of H_2S on CO_2 corrosion investigated by using EIS technique, NACE Corrosion/2005 paper n°630, Houston, TX (USA) 3-7 April (2005).
[7] B.R. Linter and G.T. Burstein, Reactions of pipeline steels in carbon dioxide solutions, Corrosion Science 41 (1999) 117-139.
[8] D.R. Morris, L.P. Samplaleanu, and D.N. Veysey, The corrosion of steel by aqueous solutions of hydrogen sulfide, Journal of the Electrochemical Society 127 (1980) 1223-1235.
[9] S. Nesic, N. Thevenot, J.L. Crolet, and D.M. Drazic, Electrochemical properties of iron dissolution in the presence of CO2 - Basics revisited, NACE Corrosion/96 paper n°3 Denver, CO (USA) 24-29 March (1996).
[10] G. Schmitt and B. Rothman, Studies of the corrosion mechanism of unalloyed steels in oxygen-free carbon dioxide solutions. Part I. Kinetics of the liberation of hydrogen, Werkstoffe und Korrosion 28 (1977) 816-822.
[11] G. Schmitt, Fundamental aspects of CO_2 corrosion, NACE Corrosion/83 paper n°43, Anaheim, CA (USA) 18-22 April (1983)..
[12] W. Schwenk, Corrosion of unalloyed steel in oxygen-free carbonic acid solutions, Werkstoffe und Korrosion 25 (1974) 643.
[13] S.N. Smith and M.W. Joosten, Corrosion of carbon steel by H_2S in CO_2 containing oilfield environments, NACE Corrosion/2006 paper n°115, San Diego, CA (USA) 12-16 March (2006).
[14] E. Remita, B. Tribollet, E. Sutter, V. Vivier, F. Ropital, and J. Kittel, Hydrogen evolution in aqueous solutions containing dissolved CO_2: Quantitative contribution of the buffering effect, Corrosion Science 50 (2008) 1433-1440.
[15] T. Tran, B. Brown, S. Nesic, and B. Tribollet, Investigation of the mechanism for acetic acid corrosion of mild steel, Corrosion/2013 paper n°2487, Orlando, FL (USA) 17-21 March (2013).
[16] Z.A. Iofa, V.V. Batrakov, and Cho-Ngok-Ba, Influence of anion adsorption on the action of inhibitors on the acid corrosion of iron and cobalt, Electrochimica Acta 9 (1964) 1645-1653.
[17] B. Le Boucher, Catalytic action of HS^- chemisorbed ions on iron in corrosion processes, 4th International Congress on Metallic Corrosion 550-555, Amsterdam (The Netherlands) (1972)
[18] D.W. Shoesmith, P. Taylor, M.G. Bailey, and D.G. Owen, The Formation of ferrous monosulfide polymorphs during the corrosion of iron by aqueous hydrogen-sulfide at 21-Degrees-C, Journal of the Electrochemical Society 127 (1980) 1007-1015.
[19] W. Sun and S. Nesic, A mechanistic model of uniform hydrogen sulfide/carbon dioxide corrosion of mild steel, Corrosion 65 (2009) 291-307.
[20] R. Galvan-Martinez, J. Mendoza-Flores, R. Duran-Romero, and J. Genesca, Effect of turbulent flow on the anodic and cathodic kinetics of API X52 steel corrosion in H_2S containing solutions. A rotating cylinder electrode study, Materials and Corrosion 58 (2007) 514-521.
[21] J. Kittel, F. Ropital, F. Grosjean, E.M.M. Sutter, and B. Tribollet, Corrosion mechanisms in aqueous solutions containing dissolved H_2S. Part 1: Characterisation of H_2S reduction on a 316L rotating disc electrode, Corrosion Science 66 (2013) 324-329.
[22] Y. Zheng, B. Brown, and S. Nesic, Electrochemical study and modeling of H_2S corrosion of mild steel, NACE Corrosion/2013 paper n°2406, Orlando, FL (USA) 17-21 March (2013).
[23] E. Remita, B. Tribollet, E. Sutter, F. Ropital, X. Longaygue, J. Kittel, C. Taravel-Condat, and N. Desamais, A kinetic model for CO_2 corrosion of steel in confined aqueous environments, Journal of the Electrochemical Society 155 (2008) C41-C45.

[24] M. Nordsveen, S. Nesic, R. Nyborg, and A. Stangeland, A mechanistic model for carbon dioxide corrosion of mild steel in the presence of protective iron carbonate films - Part 1: Theory and verification, Corrosion 59 (2003) 443-456.
[25] V.G. Levich, Physicochemical Hydrodynamics, Prentice Hall, Englewood Cliffs, New Jersey (1962).
[26] J.L. Crolet and M.R. Bonis, Revisiting hydrogen in steel, part I: theoretical aspects of charging, stress cracking and permeation, NACE Corrosion/2001 paper n°67, Houston, TX (USA) 11-16 March (2001).
[27] J.L. Crolet, Mechanisms of uniform corrosion under corrosion deposits, Journal of Materials Science 28 (1993) 2589-2606.
[28] J.L. Crolet, The electrochemistry of corrosion beneath corrosion deposits, Journal of Materials Science 28 (1993) 2577-2588.

Figure captions

Fig 1 : *Stationary cathodic polarization curves measured with a RDE at pH4 in 9 mbar H_2S saturated solution for a rotation speed of 600 rpm. The simulated points are obtained by solving the set of three differential equations (7).*

Fig 2 : *Stationary cathodic polarization curves measured with a RDE at 180 rpm in de-aerated solution containing different amount of H_2S at pH 4. The simulated points are obtained by solving the set of three differential equations (7).*

***Fig 3**: Stationary cathodic polarization curves measured with a RDE at 180 rpm in de-aerated solution containing different amount of H_2S at pH 6. The simulated points are obtained by solving the set of three differential equations (7).*

Fig 4: *Experimental stationary cathodic polarization curves measured with a RDE at different rotation speed in de-aerated solution containing at pH 6 with 50 mbar H_2S.*

Fig 5: *Evolution of the limiting cathodic current with the rotation speed of the electrode in de-aerated solution at pH 6 with 50 mbar H_2S. The line represents the theoretical Levich law for H_2S and the different square the simulated points with different values of the parameter k_1.*

Fig 6: *Variation of the limiting current in function of the k_1 value for a solution at pH 6 with 50 mbar H_2S and a rotation speed of 180 rpm.*

Fig 7: *Concentration profiles for the three species in mixed kinetic (E=-0.83, pH = 4, Ω = 180 rpm, P_{H_2S} = 9 mbar)*

Fig 8: *Concentration profiles according to the normal dimensionless distance to the electrode for a potential corresponding to the limiting current plateau of H_2S.(pH = 4, Ω = 1200 rpm, P_{H_2S} = 1 mbar)*

Fig 9: *Concentration profiles of H_2S for different k_1 values.(pH = 6, Ω = 180 rpm, P_{H_2S} = 50 mbar)*

Table caption

Table 1: *Values of the constant used for the calculation (T = 25°C). Remark the difference between the value of* k_{H^+} *given in this table and in [1] is due to the difference of reference electrode used in [1] (SSE and in the present work (Ag/AgCl).*

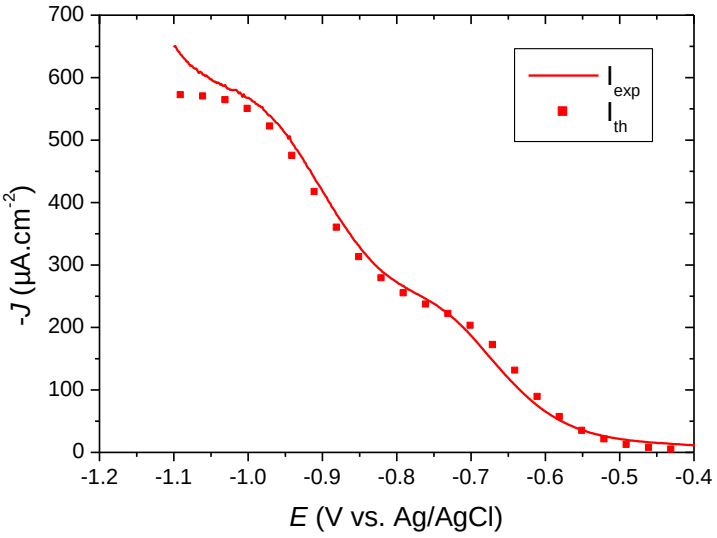
700
600
500
400
300
200
100
0
-J (µA.cm-2)
-1.2
-1.1
-1.0
-0.9
-0.8
-0.7
-0.6
-0.5
-0.4
E (V vs. Ag/AgCl)
Iexp
Ith

Figure 1

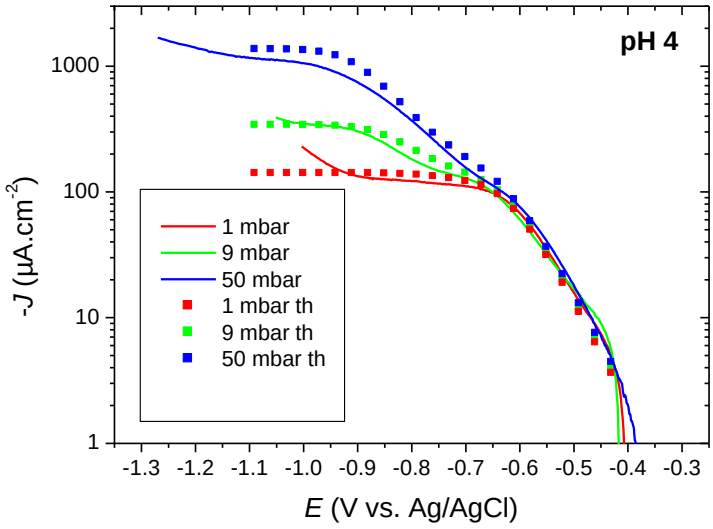
pH 4
1000
100
10
1
-J (µA.cm-2)
1 mbar
9 mbar
50 mbar
1 mbar th
9 mbar th
50 mbar th
-1.3 -1.2 -1.1 -1.0 -0.9 -0.8 -0.7 -0.6 -0.5 -0.4 -0.3
E (V vs. Ag/AgCl)

Figure 2

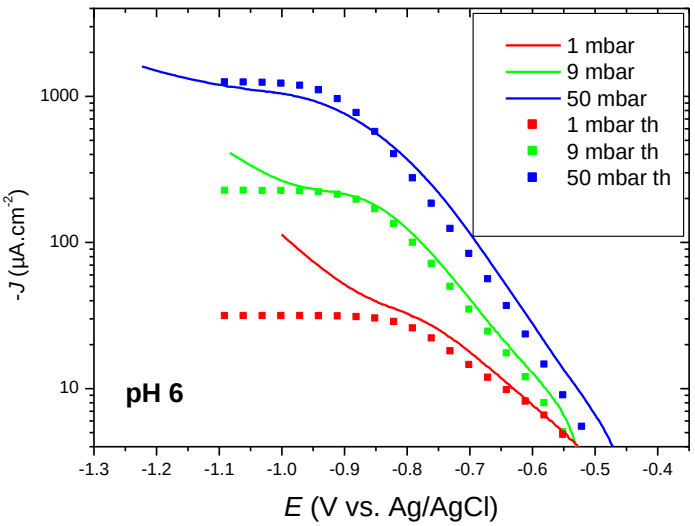
1 mbar
9 mbar
50 mbar
1 mbar th
9 mbar th
50 mbar th
pH 6
-J (µA.cm-2)
1000
100
10
-1.3
-1.2
-1.1
-1.0
-0.9
-0.8
-0.7
-0.6
-0.5
-0.4
E (V vs. Ag/AgCl)

Figure 3

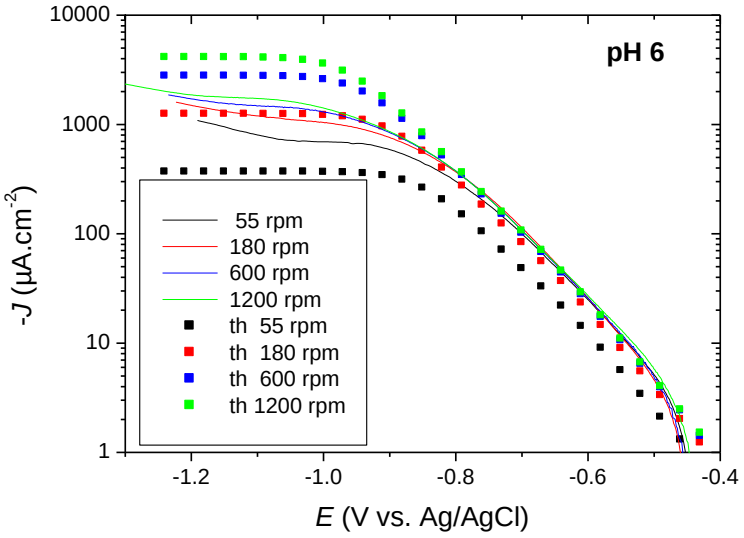
pH 6
10000
1000
100
10
1
-J (µA.cm-2)
-1.2
-1.0
-0.8
-0.6
-0.4
E (V vs. Ag/AgCl)
55 rpm
180 rpm
600 rpm
1200 rpm
th 55 rpm
th 180 rpm
th 600 rpm
th 1200 rpm

Figure 4

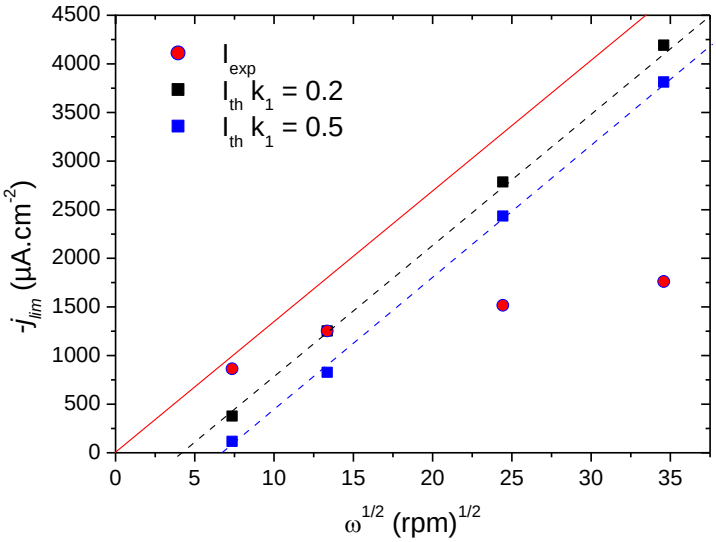
4500
4000
3500
3000
2500
2000
1500
1000
500
0
0
5
10
15
20
25
30
35
I_{exp}
I_{th} k_1 = 0.2
I_{th} k_1 = 0.5
$-j_{lim}$ (µA.cm^{-2})
$\omega^{1/2}$ (rpm)$^{1/2}$

Figure 5

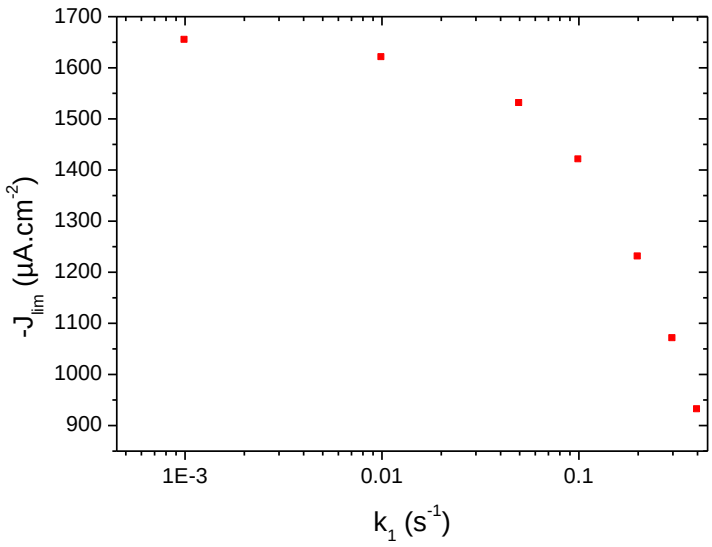
1700
1600
1500
1400
1300
1200
1100
1000
900
-J_lim (µA.cm^-2)
1E-3
0.01
0.1
k_1 (s^-1)

Figure 6

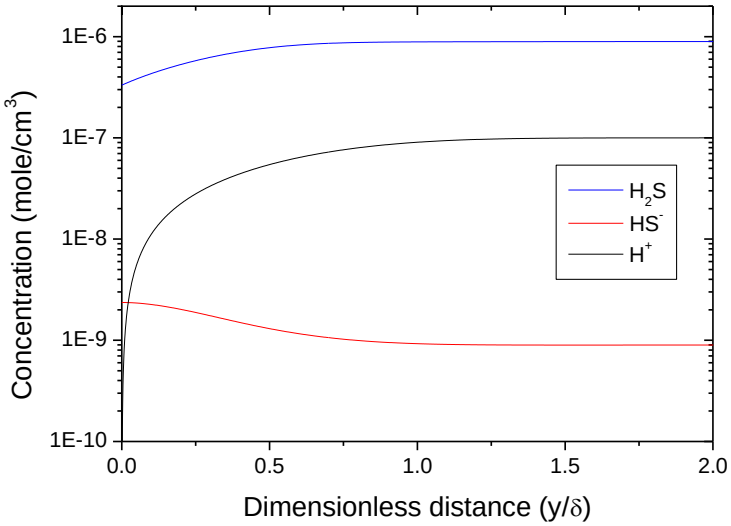
1E-6
1E-7
1E-8
1E-9
1E-10
Concentration (mole/cm3)
0.0
0.5
1.0
1.5
2.0
Dimensionless distance (y/δ)
H2S
HS-
H+

Figure 7

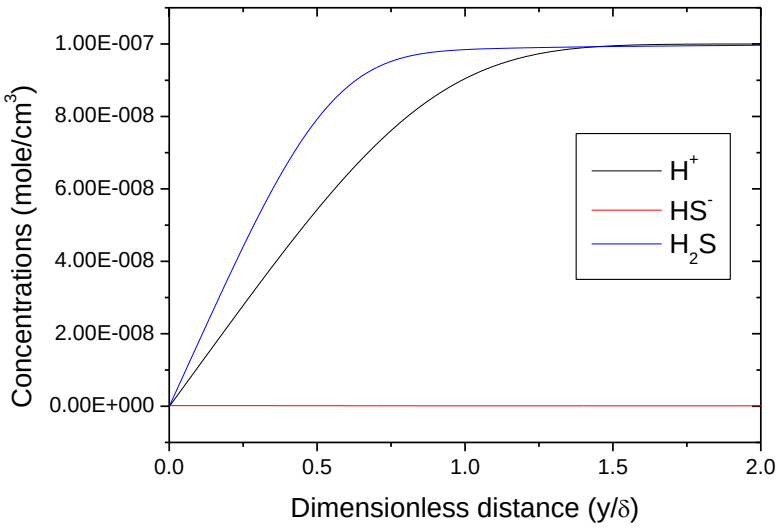
1.00E-007
8.00E-008
6.00E-008
4.00E-008
2.00E-008
0.00E+000
Concentrations (mole/cm3)
0.0
0.5
1.0
1.5
2.0
Dimensionless distance (y/δ)
H+
HS-
H2S

Figure 8

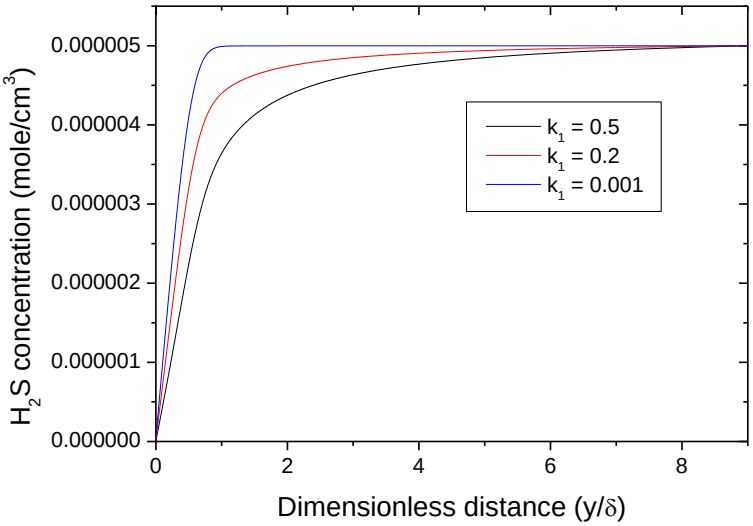
0.000005
0.000004
0.000003
0.000002
0.000001
0.000000
0
2
4
6
8
H2S concentration (mole/cm3)
Dimensionless distance (y/δ)
k1 = 0.5
k1 = 0.2
k1 = 0.001

Figure 9

Constant	Value	References
ν	0.01 cm^2s^{-1}	
D_{H^+}	9.3 x 10^{-5} cm^2s^{-1}	[6]
D_{H_2S}	1.6 x 10^{-5} cm^2s^{-1}	[6]
D_{HS^-}	2 x 10^{-5} cm^2s^{-1}	[6]
k_{H^+}	3 x 10^{-11} $mol^{0.5}cm^{-0.5}s^{-1}$	[1]
k_{H_2S}	6 x 10^{-12} $mol^{0.5}cm^{-0.5}s^{-1}$	This study
b_{c,H^+}	120 mV	[6]
b_{c,H_2S}	145 mV	[1]
k_1	0.2 s^{-1}	This study
$K_1 = \frac{k_1}{k_{-1}}$	10^{-10} mol cm^{-3}	[7]
K_2	10^{-22} à 10^{-15}	[7]

Table 1